ARTICLE

Check for updates

Journal of
Sensor Science and Technology

The Korean Sensors Society

Design and Fabrication of a High-Temperature Stable, Low-Power Microheater for Semiconductor Gas Sensors

Jun Hyeok Lee[1,2,*], Tae Won Ha[1,*], Chil-Hyoung Lee[1,+], and Dong-Weon Lee[2,3,4,+]

[1]*National Center for Nano Process & Equipments, Korea Institute of Industrial Technology (KITECH), Republic of Korea*
[2]*MEMS and Nanotechnology Laboratory, School of Mechanical Engineering, Chonnam National University, Republic of Korea*
[3]*Advanced Medical Device Research Center for Cardiovascular Disease, Chonnam National University, Republic of Korea*
[4]*Center for Next-generation Sensor Research and Development, Chonnam National University, Republic of Korea*

Cite This: *J. Sens. Sci. Technol. Vol. 35, No. 1 (2026) 22-29*

https://doi.org/10.46670/JSST.2026.35.1.22

ABSTRACT: This study presents the design, fabrication, and characterization of a Micro-Electro-Mechanical System (MEMS)-based microheater optimized for low-power portable metal-oxide semiconductor (MOS) gas sensors. To achieve enhanced mechanical stability and superior thermal isolation, a single-layer platinum (Pt) heating element was integrated onto a low-stress $SiO_2/Si_3N_4/SiO_2$ composite membrane. The fabrication process employed a multi-step Cl_2/Ar-based inductively coupled plasma (ICP) dry etching technique, which enabled high-fidelity patterning of thick Pt films. Subsequently, a Bosch-process-based deep reactive ion etching (D-RIE) technique was utilized to realize a fully suspended circular membrane architecture. Thermal evaluation demonstrated that the fabricated microheater maintains stable operation up to 400°C with a power consumption of only 99.6 mW. Infrared thermal mapping confirmed a uniform temperature distribution with less than 2% variation across a 6-inch wafer, validating the high thermal efficiency and excellent process reproducibility of the proposed design. These results establish the microheater platform as a robust and scalable solution for next-generation portable MOS gas sensing applications requiring minimized power consumption.

KEYWORDS: *Microheater, Low-power design, High-temperature stability, Semiconductor gas sensor, MEMS technology*

1. INTRODUCTION

Metal-oxide semiconductor (MOS) gas sensors are widely employed in portable and miniaturized sensing platforms owing to their high sensitivity, robustness, and compatibility with standard semiconductor fabrication processes. A critical requirement for achieving high-performance MOS gas sensors is precise and stable temperature control under low-power operation, as sensor response, selectivity, and long-term stability are primarily governed by thermally activated surface reactions [1-3]. Therefore, reliable thermal operation optimized for specific sensing materials and target gases is essential, rather than simply maintaining a constant operating temperature [4-6].

To meet these requirements, MEMS-based microheaters have been extensively integrated into MOS gas sensing platforms. Typical MOS gas sensors operate at elevated temperatures in the range of 200–400°C, with reported power consumption varying from several tens to several hundreds of mW depending on heater geometry, membrane structure, and thermal isolation efficiency [7-11]. However, simultaneously achieving low power consumption, mechanical stability, and temperature uniformity remains a significant challenge. Conventional microheater designs, particularly multilayer and thin-film configurations, are susceptible to thermally induced stress and deformation during high-temperature operation, which degrades device reliability and sensing performance [12]. Moreover, continued device miniaturization often necessitates reduced heater linewidths, leading to limited cross-sectional areas, non-uniform heat distribution, and unstable temperature control, which ultimately affects sensor response reproducibility [13].

To address these issues, various heater geometry

*These authors contributed equally to this work.
+Corresponding authors: chlee0901@kitech.re.kr (C.-H. Lee), mems@jnu.ac.kr (D.-W. Lee)
Received : Jan. 7, 2026, Revised : Jan. 11, 2026, Accepted : Jan. 20, 2026

This is an Open Access article distributed under the terms of the Creative Commons Attribution Non-Commercial License (https://creativecommons.org/licenses/by-nc/3.0/) which permits unrestricted non-commercial use, distribution, and reproduction in any medium, provided the original work is properly cited.

optimization strategies have been explored. Filipovic analyzed the effects of rounded-corner geometries and heater thickness on stress distribution and thermal performance, demonstrating that rounded corners reduce stress concentration and improve structural stability. Conversely, thinner heaters suffer from degraded temperature uniformity and require higher current densities, resulting in increased tensile stress and reduced reliability [14]. In addition, circular heater geometries have been reported to suppress edge-related heat loss more effectively than conventional rectangular designs, thereby improving thermal efficiency and temperature uniformity [15,16]. Despite these advances, most existing studies focus primarily on geometric optimization and do not sufficiently address the fabrication challenges associated with thick metal heaters and the scalable membrane formation required for low-power operation.

In single-layer microheater configurations, where the heater and electrodes are patterned on the same plane, the choice of heating material is critical for oxidation resistance, electrical stability, and fabrication reliability at high temperatures. Various metals, including Au, Al, W, and Pt, have been investigated [17]. Among these, platinum (Pt)is particularly attractive due to its high melting point, excellent oxidation resistance, minimal resistance drift, and high current density tolerance [18]. However, Pt presents significant fabrication challenges. Its chemical inertness makes both wet and dry etching difficult, while conventional lift-off processes often suffer from “wing-tip” formation, poor adhesion to silicon substrates, and hillock formation during thermal annealing. These issues become increasingly severe with thicker Pt films, limiting pattern fidelity, scalability, and long-term reliability [19].

Several Pt patterning approaches have been proposed to mitigate these limitations, including modified lift-off techniques and hard-mask-based processes [20-22]. For example, Tong et al. introduced a modified lift-off method using an SiO_2 undercut structure prior to Ti/Pt deposition, which suppressed wing-tip formation and improved pattern definition [23]. Nevertheless, such methods require additional processing steps and offer a narrow process window between metal thickness and undercut depth, restricting their applicability to thick Pt films and complex heater geometries. Consequently, reliable and scalable patterning of thick Pt microheaters remains an unresolved challenge. In parallel, membrane-based structures have been widely explored to enhance thermal isolation and reduce power consumption. Prasad et al. reported that device yield could be increased to approximately 80% by employing a sequential wet–dry etching process, compared with about 20% for wet etching alone [24]. However, approaches relying heavily on wet etching limit precise control over membrane geometry due to crystallographic etching characteristics, which restricts the realization of circular membrane structures.

In this work, a MEMS-based single-layer circular microheater is proposed to address these material and fabrication limitations. The microheater is designed for MOS gas sensor operation in the target temperature range of 200–400°C and is implemented on a low-stress $SiO_2/Si_3N_4/SiO_2$ composite membrane to enhance mechanical stability. A key contribution of this study is the introduction of a multi-step, repetitive Cl_2/Ar-based ICP dry etching process, which enables precise patterning of thick Pt films while minimizing plasma-induced damage and thermal accumulation. This approach provides improved pattern fidelity and process scalability compared with previously reported Pt patterning techniques. Furthermore, a fully circular suspended membrane structure is realized using a Bosch-process-based deep reactive ion etching (D-RIE) technique, enabling precise control over membrane geometry and effective suppression of heat dissipation to the substrate. Compared with conventional wet-etched or bridge-type membrane structures, this design significantly enhances thermal efficiency. The fabricated microheater demonstrates stable operation up to 400°C with a power consumption of 99.6 mW and exhibits less than 2% temperature variation across a 6-inch wafer, confirming excellent thermal performance and process reproducibility. These results establish the proposed microheater as a low-power, mechanically stable, and fabrication-reliable thermal platform suitable for next-generation portable MOS gas sensing systems.

2. EXPERIMENTAL SECTION

2.1 Design and Fabrication Overview of the MEMS Platform

The fabrication process of the MEMS platform for semiconductor gas sensor development is schematically illustrated in Fig. 1, while the corresponding top-view design layouts are shown in Fig. 2. An oxide/nitride/oxide (O/N/O) insulating stack was employed to provide effective electrical insulation, stress compensation, and thermal isolation between the silicon substrate and the microheater layer, enabling stable high-temperature operation. To achieve low power consumption, the overall device footprint was miniaturized to 1.2 mm × 1.2 mm. The suspended membrane region accommodating the microheater was designed with a diameter of 640 μm, while the active microheater area was defined with a diameter of 300 μm. The MEMS gas sensor platform was designed using AutoCAD, with the base unit cell corresponding to the full device area. Based on the top-view layout, individual photomasks were generated for each structural and functional layer, including the insulating layer, microheater, and electrode patterns. The MEMS

ⓒ The Korean Sensors Society

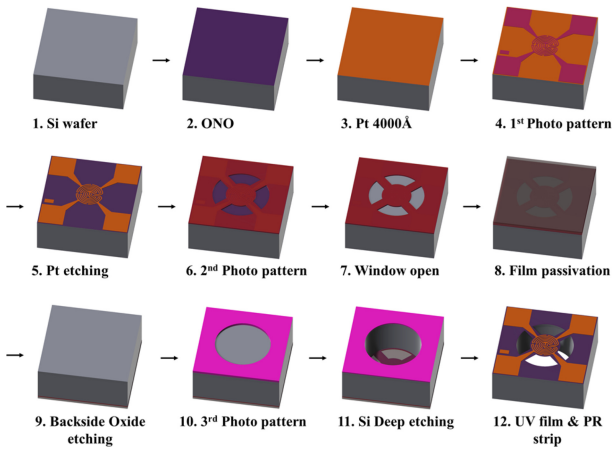

Fig. 1. Schematic illustration of the fabrication process flow of the MEMS microheater device, showing substrate preparation, thin-film deposition, photolithographic patterning of the heater structure, backside processing, deep silicon etching, and the final suspended microheater configuration.

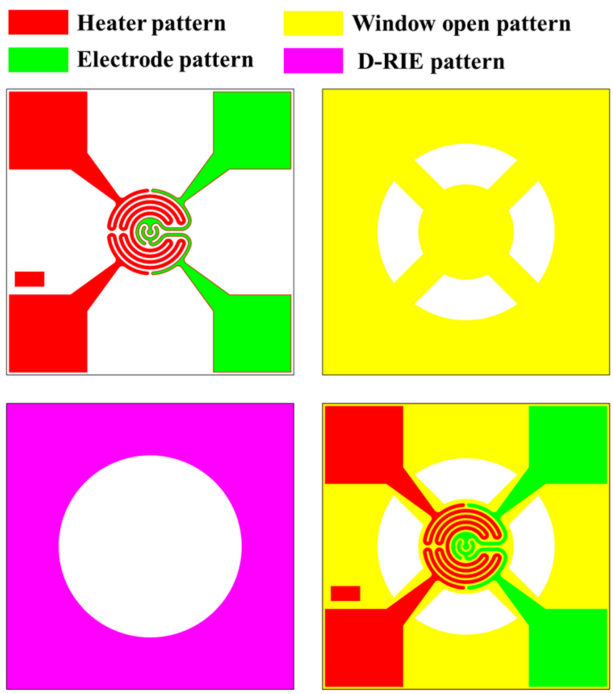

Fig. 2. Top-view schematic layouts of the MEMS microheater at different fabrication and patterning stages, illustrating the evolution of the heater geometry, electrode configuration, and membrane opening design.

platform was realized using a surface micromachining approach on a p-type (100) silicon substrate. The insulating layer, microheater thin film, and electrode structures were sequentially formed on the front side of the wafer, followed by backside silicon micromachining to define the suspended membrane structure. This design and fabrication strategy enables precise pattern definition and compatibility with subsequent processing steps, providing a robust foundation for low-power, thermally efficient gas sensor operation.

2.2 Fabrication of the MEMS Platform and Microheater

The MEMS micro gas sensor platform was fabricated on a p-type (100)-oriented silicon wafer. A low-stress oxide/nitride/oxide (ONO) insulating layer was first deposited to serve as both the membrane base and an etch-stop layer during backside micromachining. The ONO layer, with a total thickness of 1 μm, was deposited using low-pressure chemical vapor deposition (LP-CVD), providing effective electrical insulation, mechanical stability, and thermal isolation. For microheater and electrode formation, platinum (Pt), a high-resistance material suitable for microheater applications, was deposited by sputtering at 300°C. A subsequent high-temperature post-annealing process was performed to improve film stability and electrical performance. The Pt layer was patterned into microheater and electrode structures using standard photolithography. A positive photoresist (DPR-i5500) was spin-coated, followed by ultraviolet (UV) exposure and development. The exposed Pt film was selectively etched using an inductively coupled plasma (ICP) dry etching system (PlasmaLab System 133) to define the desired microheater geometry. The ICP dry etching parameters used for patterning the Pt microheater and electrode structures are summarized in Table 1.

To form the suspended membrane structure, backside micromachining of the silicon substrate was performed. Photoresist was coated on the backside of the wafer and patterned using a backside alignment mask. Deep reactive ion etching (D-RIE) based on the Bosch process was employed, utilizing alternating etching and passivation cycles with SF_6 and C_4F_8 gases to achieve high anisotropy and well-defined vertical sidewalls. The corresponding D-RIE process parameters are provided in Table 2. The etching process was

Table 1. Inductively coupled plasma (ICP) dry etching process parameters for microheater and electrode patterning.

ICP power (W)	Bias power (W)	Pressure (mTorr)	Cl_2 (sccm)	Ar (sccm)
1200	250	5	15	50

Table 2. Deep reactive ion etching (D-RIE) process parameters for silicon membrane patterning.

	Source-power (W)	Bias power (W)	Pressure (mTorr)	SF_6 (sccm)	C_4F_8 (sccm)	Time (sec)
Etch	2500	54	40	400	1	1
Passivation	2500	10	40	1	300	1.7

ⓒ The Korean Sensors Society

continued until the ONO insulating layer was exposed, which functioned as an effective etch-stop layer. This approach enabled accurate control of the membrane thickness and ensured the formation of a thermally isolated, suspended microheater structure suitable for low-power gas sensing applications.

2.3 Thermal Characterization of the MEMS Platform and Microheater

The thermal response of the MEMS microheater was evaluated by measuring the surface temperature distribution as a function of the applied voltage using an infrared (IR) thermal imaging system. The experimental setup, illustrated in Fig. 3, consisted of an IR camera mounted on a fixed stand, an optical table, a precision sample holder, an adjustable alignment stage, and a control computer. Prior to data acquisition, the microheater samples were carefully aligned under bias conditions to ensure consistent positioning relative to the IR camera, and the camera focus was optimized to clearly resolve the heater geometry. Thermal measurements were conducted under steady-state conditions; after each voltage increment, the applied bias was maintained for approximately 10 s to allow thermal stabilization before recording temperature data. All thermal characterizations were performed prior to the deposition of the gas-sensitive layer to isolate the intrinsic thermal behavior of the MEMS platform from material-dependent effects. Although accurate IR thermography ideally requires layer-specific emissivity calibration, the small dimensions and multilayer structure of the micro-platform made individual emissivity assignment impractical. To ensure measurement consistency, an emissivity value of 0.8 was uniformly applied to all infrared thermography measurements. As the microheaters were fabricated using identical materials and processes, emissivity variations among samples are negligible, and the temperature data were used for relative comparison of thermal performance rather than for absolute temperature determination. Accordingly, any systematic error resulting from the fixed emissivity assumption does not affect the comparative analysis. To improve statistical reliability, a total of six microheaters were characterized, including six devices selected from different locations on a single 6-inch wafer. Surface temperature measurements were carried out over an applied voltage range of 0~5 V, with voltage increments of 0.1 V, enabling detailed analysis of the temperature-voltage relationship and thermal uniformity of the microheater.

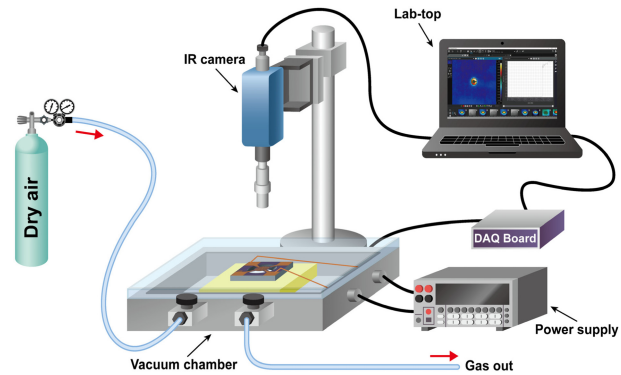

Fig. 3. Schematic illustration of the experimental setup for thermal characterization of the MEMS microheater, showing the infrared (IR) thermal imaging camera, sample stage with vacuum chuck, probe connections, DC power supply, and control laptop used for temperature–voltage measurements.

3. RESULTS AND DISCUSSIONS

3.1 Pt Etching Characteristics

To fabricate integrated microheater and electrode structures for the MEMS gas sensor platform, a 400 nm-thick platinum (Pt) thin film was patterned using photolithography followed by dry etching. Due to the high chemical inertness of Pt and the absence of volatile reaction byproducts in conventional plasma environments, Pt is widely recognized as a challenging material for plasma-based dry etching. To address this limitation, a Cl_2/Ar mixed-gas ICP etching process was employed, enabling simultaneous chemical etching and physical sputtering. The Pt etching results are summarized in Fig. 4. The ICP-RIE system used for Pt patterning is shown in Fig. 4(a) (Oxford Instruments, PlasmaLab System 133), while Fig. 4(b) illustrates the schematic process flow, in which a positive photoresist (PR) mask defines the microheater geometry on a Pt/ONO/Si substrate. The etching process was carried out using Cl_2 (15 sccm) and Ar (50 sccm) gases to achieve a synergistic etching mechanism. To suppress PR degradation and maintain etch selectivity, the process was divided into 14 repeated cycles, each including an intermediate cooling step. Under these conditions, the Pt etch rate was measured to be 9.52 Å s^{-1}, with a selectivity ratio of 0.36:1 relative to the PR mask, which was sufficient to complete Pt patterning without mask failure. As shown in Fig. 4(c) and Fig. 4(d), optical microscopy and SEM images confirm that the fabricated microheater retained its designed line width and geometry after etching. The etched Pt structures exhibited near-vertical sidewalls without noticeable undercutting, indicating effective control of lateral etching. Importantly, no damage to the underlying ONO insulating layer was observed, ensuring electrical isolation and structural

ⓒ The Korean Sensors Society

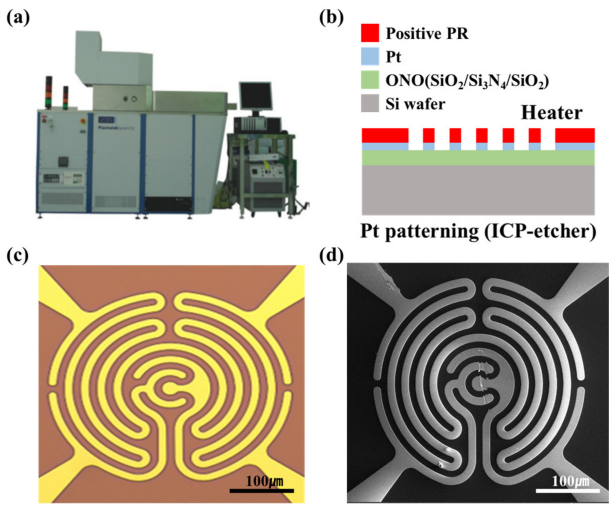

Fig. 4. Pt microheater patterning on an ONO/Si substrate using ICP dry etching: (a) ICP-RIE system employed for Pt etching (Oxford Instruments, PlasmaLab System 133); (b) schematic illustration of the Pt microheater patterning process; (c) optical microscope image of the patterned Pt microheater after etching; and (d) scanning electron microscope (SEM) image showing the detailed microheater geometry after etching.

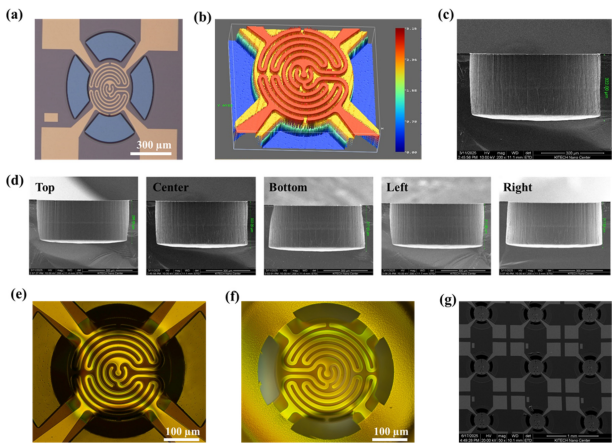

Fig. 5. Fabrication results of the MEMS-based microheater with a suspended membrane structure: (a) optical microscope image after window opening to define the bridge structure; (b) three-dimensional surface profile of the patterned structure; (c) cross-sectional SEM image after deep silicon etching; (d) SEM images acquired at five different positions (top, center, bottom, left, and right) to evaluate etch uniformity across the wafer; (e, f) optical microscope images of the released membrane structure from the front-side and back-side views, respectively; and (g) SEM image of the fully released MEMS microheater array.

integrity. During the removal of the passivation film used in the platform fabrication process, no delamination or peeling of the ONO layer was detected. In addition, optical microscope images, three-dimensional surface profiles, and SEM images acquired after Pt etching (Figs. 4 and 5) confirm that the ONO insulating layer remained intact without observable cracking or delamination, indicating that the Pt etching process did not adversely affect the ONO layer. These results demonstrate that the multi-cycle Cl_2/Ar ICP dry etching strategy enables high-resolution and reproducible micro-patterning of Pt thin films, making it well suited for the fabrication of microheaters and electrodes in high-performance MEMS gas sensor platforms.

3.2 MEMS-Based Fabrication of a Suspended Microheater Membrane

To realize a thermally isolated and mechanically stable microheater structure, a suspended membrane-type microheater was fabricated using a MEMS-based micromachining process. Fig. 5(a) shows an optical microscope image after window opening for bridge structure formation. Following Pt patterning, the membrane window was defined using GXR-601 photoresist, and the underlying ONO insulating layer was selectively dry etched. The ONO layer, with a total thickness of 1 μm, was etched using ICP dry etching under conditions of 2000 W ICP power, 150 W bias power, 14 mTorr chamber pressure, and CF_4 gas flow of 50 sccm, resulting in an average etch rate of approximately 27.8 Å s^{-1}. The three-dimensional surface profile shown in Fig. 5(b) confirms precise window formation without damage to the Pt heater or electrode structures, providing a stable membrane base for subsequent silicon etching. Backside silicon removal was performed using deep reactive ion etching (D-RIE) based on the Bosch process. A 14.2 μm-thick etch mask was patterned using JSR THB-126N photoresist to ensure high etch durability. The alternating etch and passivation cycles were repeated 1000 times, and the etch depth was precisely controlled by utilizing the ONO layer as an etch-stop. The cross-sectional SEM image in Fig. 5(c) shows that the silicon sidewalls retained a near-vertical profile, while the suspended membrane structure containing the Pt microheater remained mechanically intact.

To evaluate wafer-scale etching uniformity, etch depths were measured at five different locations (top, center, bottom, left, and right) on a 6-inch wafer, as shown in Fig. 5(d). The calculated etch uniformity was approximately 93%, indicating excellent process consistency. Optical microscope images of the released membrane viewed from the front and back sides are shown in Fig. 5(e) and Fig. 5(f), respectively, confirming complete release of the suspended structure. Fig. 5(g) presents an SEM image of a fabricated microheater array, demonstrating that the process is highly reproducible at the wafer level. The resulting bridge-type Pt microheater forms a fully suspended structure with no direct thermal conduction path to the silicon substrate. This configuration effectively

ⓒ The Korean Sensors Society

minimizes heat loss, enabling rapid temperature rise and efficient low-power operation. Such enhanced thermal isolation is critical for MEMS gas sensors that require fast thermal response and precise temperature control.

3.3 Thermal Performance and Heating Characteristics

The thermal performance of the fabricated MEMS microheater platform was evaluated using infrared (IR) thermography, as summarized in Fig. 6. Six different microheater designs fabricated in this study were characterized to assess their electrical, thermal, and heating efficiency characteristics. As shown in Fig. 6(a), the current-voltage (I-V) characteristics of all microheaters exhibit stable and reproducible electrical behavior over an applied voltage range of 0~5 V, indicating reliable electrical conduction through the Pt heater structures. The corresponding temperature–voltage (T-V) characteristics are presented in Fig. 6(b). With increasing applied voltage, a clear and monotonic increase in membrane

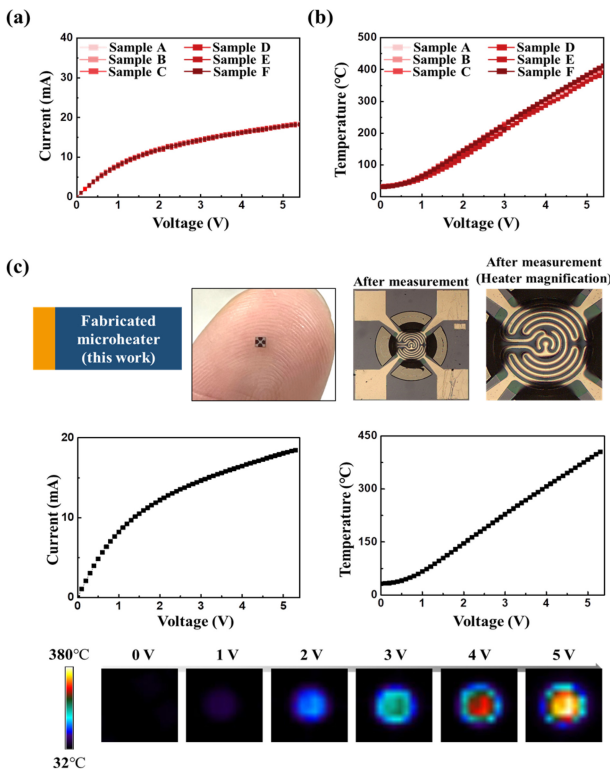

Fig. 6. Surface temperature characterization of the MEMS gas sensor platform under applied heater voltage: (a) current-voltage (I-V) characteristics of the six fabricated microheater patterns; (b) temperature-voltage (T-V) characteristics of the corresponding microheaters, highlighting differences in heating efficiency; (c) Current and temperature characteristics of the MEMS microheater platform as a function of applied voltage, and optical photographs of the fabricated microheater device and representative heater geometries.

Table 3. Power consumption and surface temperature of the fabricated MEMS microheater as a function of applied voltage.

Voltage (V)	Fabricated microheater (this work)	
	Power Consump. (mW)	Surface Temp. (°C)
1	7.93	64.2
2	23.76	144.3
3	42.93	212.3
4	64.64	306.6
5	88.65	382.4
5.3	99.6	400
6	113.94	445.8

temperature was observed for all heater designs. Above approximately 1 V, the temperature response shows an approximately linear dependence on the applied voltage, confirming stable Joule heating behavior. Minor variations in slope among the heater patterns reflect differences in heater geometry and thermal resistance, which directly influence heating efficiency. Representative optical photographs of the fabricated MEMS microheater device and the corresponding heater geometries are shown in Fig. 6(c), confirming successful realization of the designed microheater patterns on the suspended membrane platform. The power-temperature relationships derived from the electrical and thermal measurements are shown in Fig. 6(c). As the applied voltage increased, both the power consumption and surface temperature increased systematically, enabling quantitative evaluation of heating efficiency. The extracted performance metrics are summarized in Table 3.

Infrared thermal images of the microheater under increasing applied voltages are shown in Fig. 6(c). The IR images reveal that heating is strongly confined to the suspended membrane region, with negligible heat spreading to the surrounding substrate. Notably, even at operating temperatures exceeding 300°C, the thermal distribution remains uniform and localized within the membrane, confirming the effectiveness of the suspended structure in suppressing heat dissipation to the bulk silicon. The fabricated microheaters achieved a maximum operating temperature of approximately 400°C while consuming only 99.6 mW, demonstrating excellent heating efficiency. In addition, wafer-level thermal characterization revealed that performance variations among microheaters were within 2%, indicating high fabrication uniformity and process reproducibility. A comparison of the thermal performance and structural characteristics of the proposed microheater with previously reported designs is provided in Table 4. The $SiO_2/Si_3N_4/SiO_2$ composite membrane employed in this work effectively minimizes residual stress, contributing to enhanced thermal and mechanical stability compared with other membrane configurations [27-28].

ⓒ The Korean Sensors Society

Table 4. Comparison of electrothermal performance and structural characteristics of various MEMS microheater designs.

Membrane Material and Structure	Heater Geometry	Max. Temp. (°C)	Power Consump.(mW)	Device Dim. (mm^2).	Ref.
SiO_2/ Si_3N_4/SiO_2suspended membrane	Fin (Meander+Spiral)	540	120	1.2 × 1.2	Thiswork
Si_3N_4, membrane	N.S.	500	250	3.21 × 1.1	[29]
Si_3N_4, plug, membrane	N.S.	170	75	4.0 × 4.0	[30]
SiO_2/Si, suspended membrane/Microbridge	Meander	350	60	2.0 × 2.0	[31]
SiO_2/SiC, suspended membrane/Microbridge	Irregular	870	300	3.0 × 3.0	[32]
SiO_2/Si, membrane	Meander	250	120	4.0 × 4.0	[33]
SiO_2/Si, membrane	Meander	200	128	4.0 × 4.0	[34]

4. CONCLUSIONS

In this study, a single-layer, circular-patterned MEMS microheater was successfully designed and fabricated on a low-stress SiO_2/Si_3N_4/SiO_2 composite membrane to address the process complexity and thermal inefficiency commonly associated with conventional microheater architectures. A multi-step ICP dry etching strategy with short etch durations was implemented to pattern thick platinum (Pt) films, effectively suppressing plasma-induced damage and thermal accumulation while ensuring high patterning fidelity and process stability.

To enhance thermal isolation, a circular suspended membrane structure was realized through deep reactive ion etching (D-RIE), significantly reducing heat dissipation to the silicon substrate. As a result, the fabricated microheaters achieved stable operating temperatures in the range of 200–400°C with low power consumption, while maintaining a uniform temperature distribution across the active membrane region. The microheaters exhibited stable Joule heating behavior, high thermal efficiency, and excellent wafer-level uniformity, confirming the robustness and reproducibility of the proposed fabrication process. The combination of a simplified single-layer heater design and an optimized suspended membrane structure enables efficient thermal performance without sacrificing process compatibility. These results demonstrate that the proposed microheater architecture serves as a reliable and energy-efficient heat source for metal-oxide semiconductor (MOS) gas sensors. Furthermore, the structural and process strategies presented in this work are readily extendable to other MEMS-based thermal platforms, including high-temperature sensors and microsystems requiring precise temperature control.

CRediT Authorship Contribution Statement

Jun Hyeok Lee: Investigation, Conceptualization, Methodology, Writing-original draft. **Tae Won Ha:** Conceptualization, Investigation, Validation, Writing-original draft. **Chil-Hyoung Lee:** Methodology, Resources, Conceptualization, Supervision, Funding acquisition. **Dong-Weon Lee:** Supervision, Resources, Validation.

Declaration of Competing Interest

The authors declare that they have no known competing financial interests or personal relationships that could have appeared to influence the work reported in this paper.

Acknowledgements

This research was supported by Korea Evaluation Institute of Industrial Technology (KEIT) grant funded by the Korea government (MOTIE) (RS-2023-00257663) and the Korea Institute of Industrial Technology (KITECH, Project no. UR260001).

REFERENCES

[1] H. Chai, Z. Zheng, K. Liu, J. Xu, K. Wu, Y. Luo, et al., Stability of metal oxide semiconductor gas sensors: A review, IEEE Sens. J. 22 (2022) 5470–5481.
[2] A. Dey, Semiconductor metal oxide gas sensors: A review, Mater. Sci. Eng. B 229 (2018) 206–217.
[3] J. Yun, M. Cho, K. Lee, M. Kang, I. Park, A review of nanostructure-based gas sensors in a power consumption perspective, Sens. Actuators B Chem. 372 (2022) 132612.
[4] E. Martinelli, D. Polese, A. Catini, A. D'Amico, C. Di Natale, Self-adapted temperature modulation in metal-oxide semiconductor gas sensors, Sens. Actuators B Chem. 161 (2012) 534–541.
[5] A. Fort, V. Vignoli, S. Rocchi, L. Tondi, M. Serrano-Santos, M. Mugnaini, Fine tuning design of control board parameters for sensing applications, Proceedings of the IEEE Instrumentation and Measurement Technology Conference, Sorrento, Italy, 2006, pp. 2244–2248.
[6] J. Warmer, P. Wagner, M.J. Schöning, P. Kaul, Detection of triacetone triperoxide using temperature cycled metal-oxide semiconductor gas sensors, Phys. Status Solidi A 212 (2015) 1289–1298.
[7] R. Prajesh, N. Jain, A. Agarwal, Low power highly sensitive platform for gas sensing application, Microsyst.

ⓒ The Korean Sensors Society

Technol. 22 (2016) 2185–2192.
[8] T. Zhang, Z. Pan, C. Zhang, L. Xiong, C. Yang, J. Zhang, et al., Development of a microheater with a large heating area and low thermal stress in the heating area, Micromachines 15 (2024) 130.
[9] R.G. Spruit, J.T. Van Omme, M.K. Ghatkesar, H.H.P. Garza, A review on development and optimization of microheaters for high-temperature in situ studies, J. Microelectromech. Syst. 26 (2017) 1165–1182.
[10] B. Biswas, F.A. Talukdar, G.S. Baghel, Design and simulation of a microheater to increase the reusability of the gas sensor, Microsyst. Technol. 31 (2025) 3469–3482.
[11] H. Shwetha, S. Sharath, B. Guruprasad, S. Rudraswamy, MEMS based metal oxide semiconductor carbon dioxide gas sensor, Micro Nano Eng. 16 (2022) 100156.
[12] A.M. Simonyan, Y.G. Sanoyan, Investigation of the plane stress state of a multilayer structure under heat variations, Mech. Solids 44 (2009) 756–761.
[13] M. Calderon-Gonzalez, D. Cheyns, R. Ameloot, J. Genoe, Integrated sensors to experimentally measure microheater uniformity: Geometry implications in meander-based structures, J. Microelectromech. Syst. 33 (2024) 736–746.
[14] L. Filipovic, Reliability of platinum microheater geometries for MEMS-based gas sensors, Proceedings of the IEEE International Integrated Reliability Workshop (IIRW), South Lake Tahoe, USA, 2022, pp. 1–6.
[15] G. Petrucci, D. Caputo, A. Nascetti, N. Lovecchio, E. Parisi, S. Alameddine, et al., Thermal characterization of thin film heater for lab-on-chip application, Proceedings of the XVIII AISEM Annual Conference, Trento, Italy, 2015, pp. 1–4.
[16] M. Gayake, D. Bodas, S. Gangal, Simulations of polymer based microheater operated at low voltage, Proceedings of the COMSOL Conference, Bangalore, India, 2011, pp. 1–5.
[17] Z.E. Jeroish, K. Bhuvaneshwari, F. Samsuri, V. Narayanamurthy, Microheater: material, design, fabrication, temperature control, and applications—a role in COVID-19, Biomed. Microdevices 24 (2022) 3.
[18] S. Jadav, Thermal and electrical characterization of flexible microheaters: Influence of material choice and geometry, Microelectron. Reliab. 175 (2025) 115944.
[19] J.C. Park, S. Hwang, J.-M. Kim, J.K. Kim, E.-H. Kim, Y.-G. Jung, et al., High density plasma etching of platinum films in BCl_3/Ar and CF_4/Ar inductively coupled plasmas, Electron. Mater. Lett. 5 (2009) 205–208.
[20] D.A. Golosov, J. Okojie, S. Zavadski, A. Rudenkov, S. Melnikov, V. Kolos, Stability of the platinum electrode during high temperature annealing, Thin Solid Films 661 (2018) 53–59.
[21] Z. Yao, C. Wang, H.-K. Sung, N.-Y. Kim, Defined micropatterns of platinum thin films by inductively coupled plasma etching using SF_6/Ar/O_2 mixture gas, Mater. Sci. Semicond. Process. 27 (2014) 228–232.
[22] F. Samaeifar, A. Afifi, H. Abdollahi, Simple fabrication and characterization of a platinum microhotplate based on suspended membrane structure, Exp. Tech. 40 (2016) 755–763.
[23] H.D. Tong, R. Zwijze, J. Berenschot, R. Wiegerink, G. Krijnen, M. Elwenspoek, Platinum patterning by a modified lift-off technique and its application in a silicon load cell, Sens. Mater. 13 (2001) 235–246.
[24] M. Prasad, P.S. Dutta, Development of micro-hotplate and its reliability for gas sensing applications, Appl. Phys. A 124 (2018) 788.
[25] Q. Zhou, A. Sussman, J. Chang, J. Dong, A. Zettl, W. Mickelson, Fast response integrated MEMS microheaters for ultra-low power gas detection, Sens. Actuators A Phys. 223 (2015) 67–75.
[26] A. Mahdavifar, R. Aguilar, Z. Peng, P.J. Hesketh, M. Findlay, J.R. Stetter, et al., Simulation and fabrication of an ultra-low power miniature microbridge thermal conductivity gas sensor, J. Electrochem. Soc. 161 (2014) B55-B61.
[27] B. Guo, A. Bermak, P.C. Chan, G.-Z. Yan, An integrated surface micromachined convex microhotplate structure for tin oxide gas sensor array, IEEE Sensors J. 7 (2007) 1720–1726.
[28] Y. Mo, Y. Okawa, M. Tajima, T. Nakai, N. Yoshiike, K. Natukawa, Micro-machined gas sensor array based on metal film micro-heater, Sens. Actuators B Chem. 79 (2001) 175–181.
[29] A. Pike, J.W. Gardner, Thermal modeling and characterization of micropower chemoresistive silicon sensors, Sens. Actuators B Chem. 45 (1997) 19–26.
[30] D. Briand, B. van der Schoot, N.F. de Rooij, H. Sundgren, I. Lundstrom, A low power micromachined MOSFET gas sensor, J. Microelectromech. Syst. 9 (2000) 303–308.
[31] B.-U. Moon, J.-M. Lee, C.-H. Shim, M.-B. Lee, J.-H. Lee, D.-D. Lee, et al., Silicon bridge type micro-gas sensor array, Sens. Actuators B Chem. 108 (2005) 271–277.
[32] G. Wiche, A. Berns, H. Steffes, E. Obermeier, Thermal analysis of silicon carbide based micro hotplates for metal oxide gas sensors, Sens. Actuators A Phys. 123 (2005) 12–17.
[33] P. Bhattacharyya, P.K. Basu, B. Mondal, H. Saha, A low power MEMS gas sensor based on nanocrystalline ZnO thin films for sensing methane, Microelectron. Reliab. 48 (2008) 1772–1779.
[34] S. Roy, C.K. Sarkar, P. Bhattacharyya, A highly sensitive methane sensor with nickel alloy microheater on micromachined Si substrate, Solid-State Electron. 76 (2012) 84–90.

ⓒ The Korean Sensors Society